Diamond & Related Materials 162 (2026) 113207

Contents lists available at ScienceDirect

Diamond & Related Materials

journal homepage: www.elsevier.com/locate/diamond

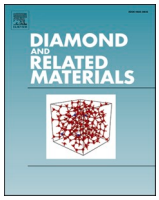

Controlled flexibility and improved tribological performance of Si/O -DLC coated rubber by reducing mechanical mismatch

Ziyu Du [a,b], Xin Zhang [b], Silong Zhang [b], Rende Chen [b], Wei Yang [b], Hao Li [b], Kazuhito Nishimura [b], Peng Guo [b,*], Aiying Wang [b,*]

[a] School of Materials Science and Chemical Engineering, Ningbo University, Zhejiang, Ningbo, 315211, China
[b] State Key Laboratory of Advanced Marine Materials, Zhejiang Key Laboratory of Extreme-environmental Material Surfaces and Interfaces, Ningbo Institute of Materials Technology and Engineering, Chinese Academy of Sciences, Ningbo, 315201, China

ARTICLE INFO

Keywords:
Rubber
Diamond-like carbon
Si/o co-doping
In-situ stretching
Finite element method

ABSTRACT

Under high-speed and heavy-load conditions, rubber sealing products suffer severe wear, leading to reduced service life of key components of equipment. Hard and wear-resistant Diamond-like carbon (DLC) coatings offer a promising solution. While, different from DLC coated rigid substrate, the elasticity and stress distribution combining interfacial deformation of DLC-coated soft substrate show notable discrepancy during tribological test, the related wear mechanism remains poorly understood. In this study, DLC with different Si and O contents (Si/O-DLC) were deposited on nitrite butadiene rubber (NBR). With Si/O content increasing from 3.05 to 8.47 at. % and 2.42 to 7.56 at.%, respectively, the stress in DLC, the hardness and elastic modulus of DLC coated rubber tended to decrease, which enhanced adhesion strength and benefited less cracks for delamination under in-situ tensile testing. Finite element method confirmed that the synergistic improved flexibility together with the reduced mismatch of mechanical properties between Si/O-DLC and NBR, subsequently avoiding stress accumulation and suppressing cracking and spallation. All these contributions enabled the low and stable friction coefficient (COF) for the Si/O-DLC coated on the rubber, specifically with COF less than 0.38 under 5 N and 10 N. The results provide an effective strategy to improve the wear resistance of hard DLC coated flexible rubber in practical working conditions.

1. Introduction

Due to its excellent flexibility and air tightness, rubber products are widely applied in numerous fields, such as automotive, aerospace, engineering and biomedical industries, especially in aero-engine hydraulic system seals, pistons and valves [1], which can effectively prevent lubricant leakage and the entry of external dust and foreign objects [2]. However, under the actual working conditions in regard to high speed and heavy load, the soft rubber often exhibits severe wear when sliding contact with other metal or ceramic engineering materials, resulting in sealing failure of some key devices and devastating disaster [3]. Therefore, to extend the service life of advanced equipment, it is of great significance to improve the wear resistance of rubber components.

Adopting wear-resistant diamond-like carbon (DLC) is considered as an extricable method, in view of its outstanding high hardness, chemical inertness, low coefficient of friction (COF) and low wear rate [4–7]. In addition, both rubber and DLC are composed of C and H elements, they should have good chemical compatibility and high adhesion strength [8,9]. Recently, many attempts have been made to explore the beneficial effects of DLC modified rubber [10–12], and the reduced wear rate and 74 % reduction of the COF have been reported [13,14].

However, the residual stress of DLC film is up to several GPa, the elastic mismatch between DLC and rubber is too large [15], the easy peeling of DLC from the rubber has to be considered for its practical application [16]. It was previously reported that Si doping can reduce the residual stress of DLC, improve its adhesion strength and flexibility [17,18], and O doping can reduce the COF of DLC [19]. So, the silicon-oxygen co-doped DLC (Si/O-DLC) may be the preferred solution. For example, with acetylene (C_2H_2) and hexamethyldisiloxane (HMDSO) precursor, Zhang et al. [20] prepared Si/O-DLC using plasma-enhanced chemical vapor deposition technique (PECVD), and found that Si/O can not only improve their thermal stability, but also significantly reduce the residual stresses. Similarly, Jiang et al. [21] found that Si/O-DLC had a high adhesion strength of $Lc_1 \sim 8.1$ N, with reducing the COF from 0.4 to

* Corresponding authors.
E-mail addresses: guopeng@nimte.ac.cn (P. Guo), aywang@nimte.ac.cn (A. Wang).

https://doi.org/10.1016/j.diamond.2025.113207
Received 28 October 2025; Received in revised form 10 December 2025; Accepted 14 December 2025
Available online 15 December 2025

0.13 and the wear rate of polyether ether ketone by ten times.

Conversely, it is widely acknowledged that, the application of hard coatings can result in a decrease in elasticity, wrinkled and folded structures on the soft substrate, which may lead to significant degradation of service performance and unpredictable tribological behavior. The main reason lies in the unavoidable interfacial deformation from the highly elastic substrate, which can induce great variations in contact area, morphology, and stress concentration characteristics at the frictional sliding interface [22,23]. While, owing to a lack of investigation on the elasticity, stress distribution and interfacial deformation characteristic during tribological testing, the wear mechanism of DLC-coated soft substrate remains poorly understood.

In this work, Si/O-DLC films were deposited on rubber by PECVD method. The Si/O content was changed by regulating the flow ratio of C_2H_2 and HMDSO. The effect of Si/O content on the morphology, structure, adhesion strength and tribological properties of Si/O-DLC films was investigated. Besides, the flexibility of the sample was evaluated by in-situ tensile testing, the stress distribution, deformation characteristic under tribological test were analyzed with the finite element method (FEM), the related wear mechanism of the DLC-coated rubber was also discussed.

2. Experimental

2.1. Film deposition

The Si/O-DLC films were prepared on rubber (NBR) (25 × 25 × 2 mm^3) and P-type Si (100) wafers using PECVD equipment in Fig. 1. During deposition, high-purity C_2H_2 with a purity of approximately 99.999 vol% and HMDSO with a purity greater than 99 vol% were used. Before fixed into the substrate holder, all substrates need to be ultrasonically pre-cleaned with anhydrous ethanol for 10 min. When the vacuum chamber was evacuated to below 2×10^{-5} Torr, the substrates were cleaned by Ar ions for 20 min, under 20 mTorr argon gas and 500 V pulse negative bias voltage. During the deposition process, the pulse negative bias voltage, the pulse power and the duty cycle were set at 450 V, 160 W and 61.5 %, respectively. The Si/O contents in the films were adjusted by regulating the flow ratio of C_2H_2 and HMDSO gas, and the process parameters were shown in Table 1. Correspondingly, the four samples were named S0, S1, S2, and S3 for various flow ratio of C_2H_2 and HMDSO. The total gas flow rates of C_2H_2 and HMDSO were 100, 110, 70, and 40 sccm, respectively. Prior to deposition, the vacuum chamber was evacuated to below 2×10^{-5} Torr. By adjusting the flow rates of the C_2H_2 and HMDSO precursors, the working pressure was consistently maintained at 3.7 ± 0.3 mTorr. By adjusting the flow rates of the C_2H_2 and HMDSO precursors, the working pressure was consistently maintained at 3.7 ± 0.3 mTorr. Additionally, meticulous control of the deposition time ensured consistent film thickness throughout the experimental process, as shown in Table 1.

2.2. Sample characterization

The film thickness was characterized using a field emission scanning electron microscope (SEM, S4800) and surface profiler (ASTQ), and the deposition rate was calculated. The surface morphology of the original samples and the wear tracks after tribological test were investigated by field emission scanning electron microscopy (FEI Quanta FEG 250).

The compositional content and chemical bonding state of the DLC films were measured by X-ray photoelectron spectroscopy (XPS, Axis UltraDLD, Japan), with Al (single Kα) photon energy of 1486.6 eV. In order to avoid the influence of oxidation and surface impurities from vacuum chamber or the surrounding atmosphere, the as-deposited films were pre-etched by Ar ion for 2 min prior to the XPS measurement. The carbon atomic bonding microstructure of the DLC films was

Table 1
Detailed process parameters of Si/O-DLC films.

Sample	C_2H_2 (sccm)	HMDSO (sccm)	Deposition time (min)
S0	100	0	25.0
S1	100	10	25.0
S2	60	10	21.5
S3	30	10	20.0

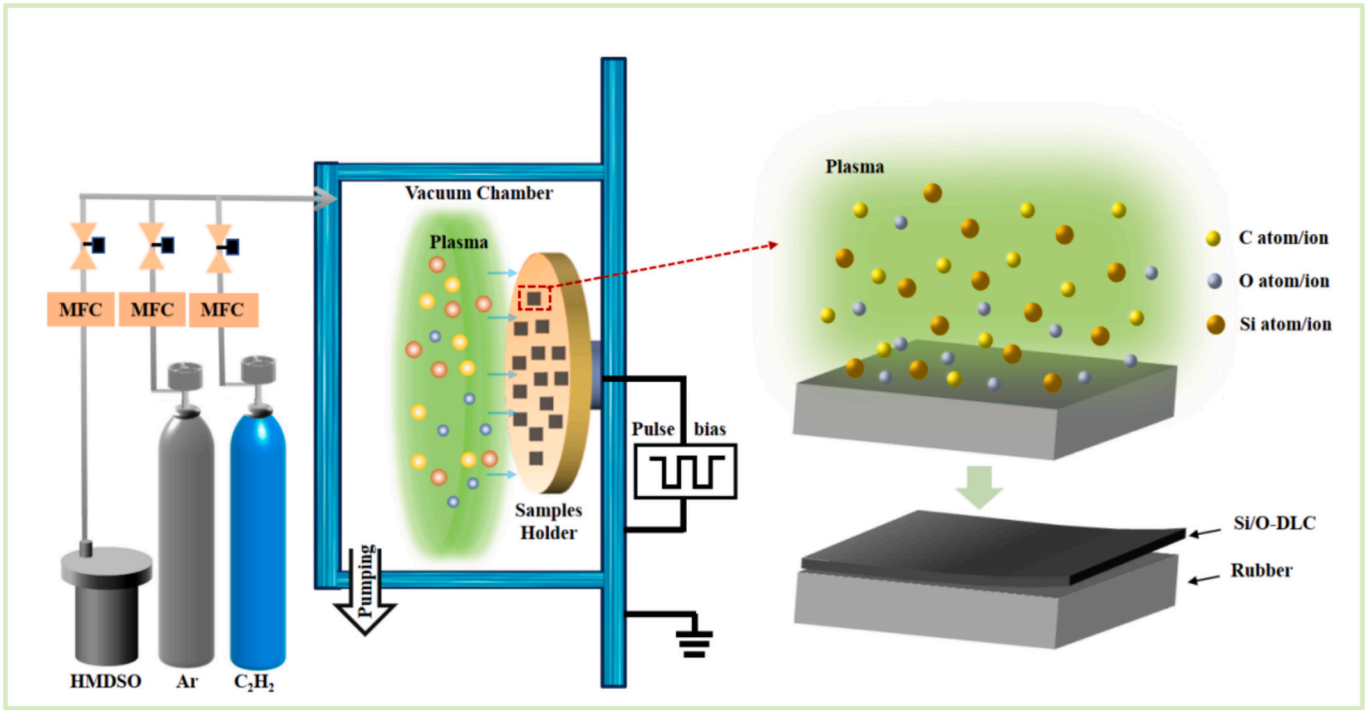

Fig. 1. Schematic diagram of PECVD system.

characterized by confocal micro-Raman spectroscopy (In Via-reflex, Renishaw), with an excitation wavelength of 532 nm and a test wavelength range of 800–2000 cm^{-1}.

The residual stress of the samples was tested using the stress tester (FST5000), where the stress was calculated by comparing the change in curvature radius of the Si substrate before and after the coating deposition. The mechanical properties of the DLC films were evaluated using the MTS nanoindentation system (G200), using the continuum stiffness method, combined with the Oliver-Pharr model [24], the hardness (H) and elastic modulus (E) of the films were calculated. To avoid the elastic deformation of rubber, the same DLC deposited on Si wafers were tested here. The measurement results were used as a reference to evaluate the H and E of DLC on rubber with different Si/O contents [25]. Six test points were randomly selected to get an averaged result.

The adhesion strength between DLC and the rubber substrate was evaluated by X-cutting method. An "X" was cut on the surface of the sample with a razor blade, and the angle of the two crossed lines was kept at 30°-45°. The adhesive tape was adhered to the position of the incision, and a load of 10 N was applied. The adhesive tape was quickly torn off from the surface of the film after 2 min, then, the flaking and delamination around the X-cutting position were observed by SEM.

By installing a tensile test bench internally, in-situ tensile testing was conducted on the sample to observe the flexibility of the coated samples during stretching process. The samples were loaded by controlling the elongation, with the maximum tensile load of 500 N and the maximum elongation of 100 % (100 %).

The tribological tests were conducted in a climate-controlled laboratory environment where both temperature and humidity were maintained at stable levels. Specifically, the temperature was kept at approximately 26 °C, and the relative humidity was maintained within the range of 50 % ± 5 %. A multifunctional friction and wear testing machine (UMT-3) was used to evaluate the wear resistance of the coated rubber. A GCr15 steel ball with a diameter of 6 mm was selected as the counterpart. The sliding speed was 5 mm/s, and the loads were 5 N and 10 N, respectively.

2.3. Finite element method model

In tribological experiments, the applied load can induce complex stress fields and large deformation in DLC-coated soft substrate. Finite element simulation can be used to figure out energy dissipation process and the principal factors affecting its tribological performance. Combined with dynamic monitoring data of contact stress fields during friction experiments, critical stress zones for crack initiation (e.g., interfacial shear stress concentration regions) and the mechanical driving forces behind failure modes, such as delamination can be confirmed. For instance, Von Mises stress contour maps can reveal the initiation sites of plastic yielding in substrate materials, which exhibits significant spatial correlation with experimentally observed plowing grooves and material transfer phenomena [26]. Furtherly, parametric simulations can enable quantitative analysis of stress peak evolution under varying load and sliding velocity conditions, thereby establishing experimental safety thresholds (e.g., critical load ranges maintaining Von Mises stress below substrate yield strength).

Specifically, the finite element software (ABAQUS 2022) was employed to simulate the stress distribution and deformation of different coating systems. With Mooney-Rivlin model for describing the mechanical behavior of rubber-like hyperelastic materials, the used material physical properties parameters are shown in Table 2 and Table 3, where C10 and C01 denote the material's shear stiffness constants, D1 represents the compressibility parameter associated with volumetric deformation.

Given the symmetry in both structural configuration and applied loading, only the right half-section of the coating/substrate system was modeled to enhance computational efficiency. As shown in Fig. 2, the thickness of the DLC was 0.5 μm, to avoid any artificial constraints or edge effects, a large substrate region with a diameter of 5 mm and a height of 2 mm was modeled. The diameter of the GCr15 ball was 6 mm. Mapped meshing with significant refinement around the contact region resulted in approximately 806,739 linear quadrilateral element (CAX4R), with a minimum element size of 2×10^{-7} mm. The boundary conditions applied are shown in Fig. 2.

Table 2
Materials properties used in finite element analyses.

Material	Young's modulus, E (GPa)	Poisson's ratio	Density (g/cm^3)	Reference
Si/O-DLC	S0-S3	0.07	2.8	[27–29]
GCr15	208	0.3	7.8	[30]

3. Results and discussion

3.1. Composition and microstructure

Fig. 3 shows the thickness and deposition rate of Si/O-DLC films with different Si/O contents. By changing deposition time, the thickness of all the samples basically remained around 500 nm. When C_2H_2 was used as the reaction gas, its deposition rate was the lowest, around 20.04 nm/min. As the gas flow ratio of HMDSO and C_2H_2 increased from 1:10 to 1:3, the corresponding deposition rate increased from 19.96 nm/min to the maximum value about 25.65 nm/min, monotonically. This growing deposition rate can be attributed to the lower ionization energy of HMDSO, and the higher HMDSO/C_2H_2 ratio caused the higher dissociation rate.

Fig. 4 shows the surface morphologies of DLC films deposited on rubber. At low magnification, random cracks were distributed on the surface of all samples, their sizes were in micrometer scale, as marked with an arrow in green. This was a typical topographical feature of rigid films on soft substrates. This morphology was characteristic of rigid films on soft substrates. The significant difference in the coefficients of thermal expansion between the rubber substrate ($\approx 1.8 \times 10^{-4}\ K^{-1}$) and the DLC films ($\approx 6 \times 10^{-6}\ K^{-1}$) led to thermal strain during processing, which was responsible for the formation of these crack networks [32].

In Fig. 4(a), corresponding to sample S0, film warping and delamination were evident along the cracks, with numerous fine film fragments remaining attached at these locations. As shown in Fig. 4(b) for sample S1, more pronounced warping and delamination occurred at the crack sites. As shown in Fig. 4(c) and (d) for sample S2 and S3, the film edges along the cracks were tilted inward. This feature was consistent with the growth behavior of DLC films under a positive temperature difference [33]. At high magnification (20000×) from the inserted images, all the DLC films achieved complete and uniform substrate coverage, and showed a typical cauliflower-like nanostructures.

Fig. 5(a) shows the C, Si and O contents of the as-deposited films. With HMDSO/C_2H_2 ratio of 1:10, 1:6 and 1:3, the Si content of S1, S2, S3 samples were 3.05, 4.25 and 8.47 at.%, and the O content were 2.42, 2.89 and 7.56 at.%, respectively.

Fig. 5(b) shows the C1s spectra of the DLC films. The peaks of sp^3-C and Si—O bonds located at 285.2 ± 0.1 eV and 286.5 ± 0.1 eV, respectively. The peak with a binding energy of 284.7 eV represented the sp^2-C or C-Si-O bonds. Fig. 5(c) presents the Si 2p spectra of all films and their fitting results. Two peaks around 100.9 ± 0.2 eV and 101.5 ± 0.2 eV, represented the Si—C and Si(—O)$_1$ bonds, respectively [34].

From Fig. 5(a) and (b), as the percentage of Si/O in the DLC film increased, the sp^3-C bond showed a decreasing trend, and on the

Table 3
Material constants of Mooney-Rivlin hyperelastic model for rubber.

Material	C10	C01	D1	Reference
Rubber	1.9519	−0.3067	0.0012	[31]

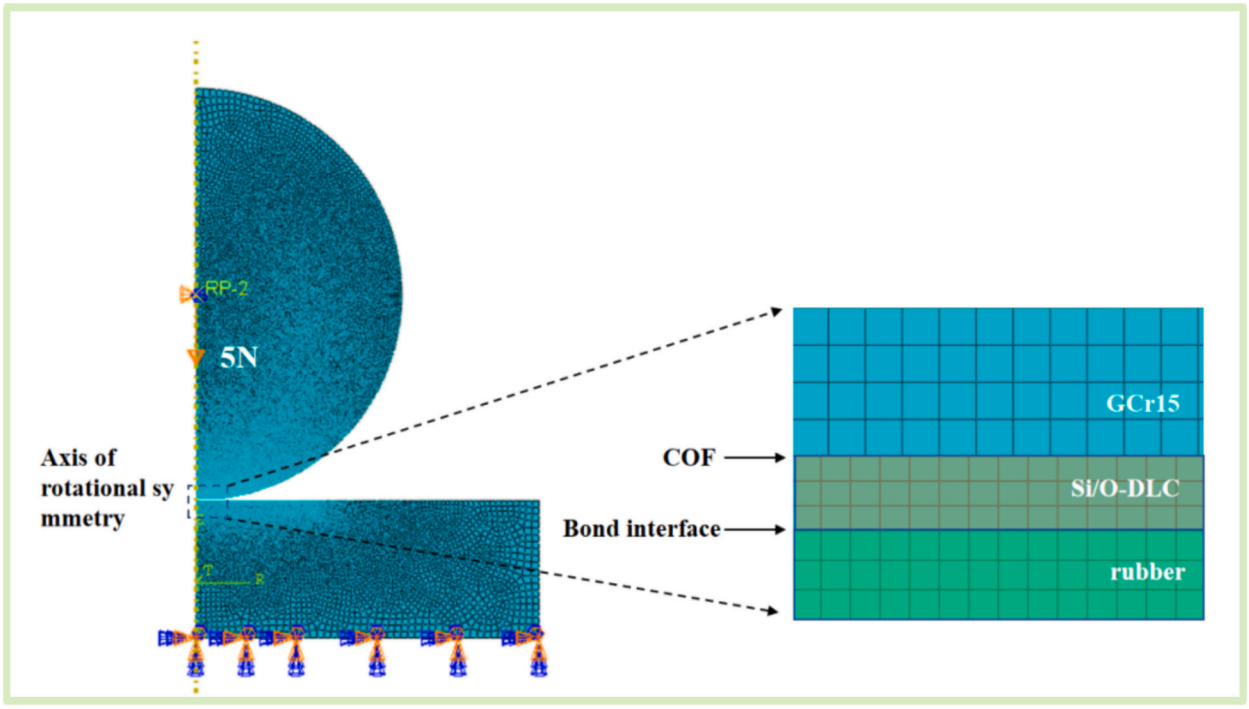

Fig. 2. Schematic of the model and mesh generation of the finite element analysis.

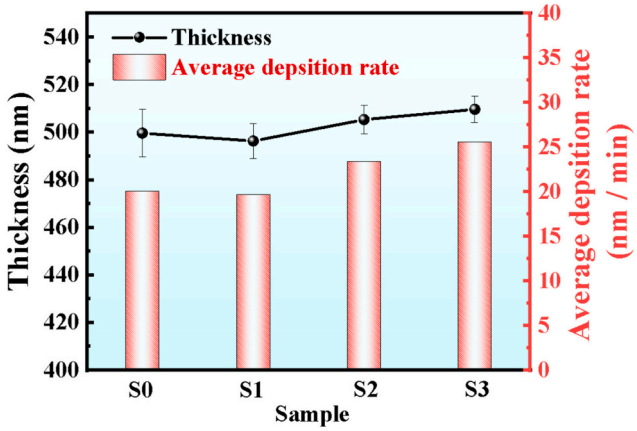

Fig. 3. The thickness and deposition rate of the films.

contrary, the sp^2-C/C-Si-O bond content increased.

In order to analyze the effect of Si/O on the bonding structure of the amorphous carbon matrix, the films were characterized by Raman spectroscopy, as shown in Fig. 6. For all the samples, the G peak was around 1530 cm^{-1} and the D peak appeared around 1350 cm^{-1}. The G peak position, the ratio of the area of G peak and D peak (I_D/I_G) and the full width at half maximum of G peak (G_{FWHM}) are shown in Fig. 6(b).

When the Si content in the film increased from 0 to 8.47 at.% and the O content increased to 7.56 at.%, the G peak position gradually decreased from 1525.42 cm^{-1} to 1518.86 cm^{-1}, suggesting the decrease in sp^3 content. I_D/I_G increased from 0.579 to 0.665, indicating the increasing size of sp^2 clusters. G_{FWHM} gradually decreased from 189.26 to 174.68 cm^{-1}, suggesting the improved ordering of the DLC film [35].

3.2. Mechanical properties

Fig. 7 presents the residual stresses of the DLC films as a function of Si/O content. With the increase of Si/O content, the residual stress showed a decreasing trend. The pure DLC film had the highest residual stress, approximately 1.4 GPa. As the Si content increased from 3.05 to 8.47 at.%, the residual stress decreased from 0.9 to 0.15 GPa. This reduction can be attributed to the formation of C-Si-O and C—Si bonds in samples S1, S2, and S3, which had lower bond energies than that of C—C bonds, thereby relaxing the internal stress. Additionally, the incorporation of Si into the amorphous carbon matrix can further contribute to stress relief [36,37].

The Fig. 7 also shows the hardness and elastic modulus of the DLC films deposited on silicon wafers. The pure DLC film exhibited the highest hardness (>20 GPa) and elastic modulus (>180 GPa), and the both mechanical property parameters decreased progressively with increasing Si/O content. It can be explained from the increase of sp^2 cluster size and the destruction of the continuity of amorphous carbon matrix by the introduction of Si and O atoms. H/E and H^3/E^2 were calculated in Fig. 7. Their H/E ratio kept stable around 0.1, while, the H^3/E^2 values showed a decreasing trend with increasing Si and O content, from 0.24 to 0.12 GPa.

3.3. Adhesion properties

In order to investigate the effect of Si/O content on the adhesion strength between DLC films with the rubber substrate, X-cutting tests were carried out. SEM of the X-cut of DLC films with different Si/O contents are shown in Fig. 8.

As shown in Fig. 8(a), the S0 sample had the worst adhesion strength, some distinct vertical stripes were found on its surface, which were related to the molding process of rubber manufacturing. Its X-cut was relatively flat and smooth without jagged structure. However, near the location of the X notch, as shown by the dashed box in Fig. 8(a), the stripes disappeared and its surface showed rough and uneven burrs, which indicated that the film peeled off from the rubber.

As shown in Fig. 8(b), the S1 sample also showed slight peeling in the dashed box near the X-cut location. In Fig. 8(b), sample S1 also showed slight peeling within the dashed box near the X-cut. In contrast, S2 and S3 demonstrated the best adhesion, with smooth and flat incision surfaces and no signs of film flaking. This behavior could be attributed to

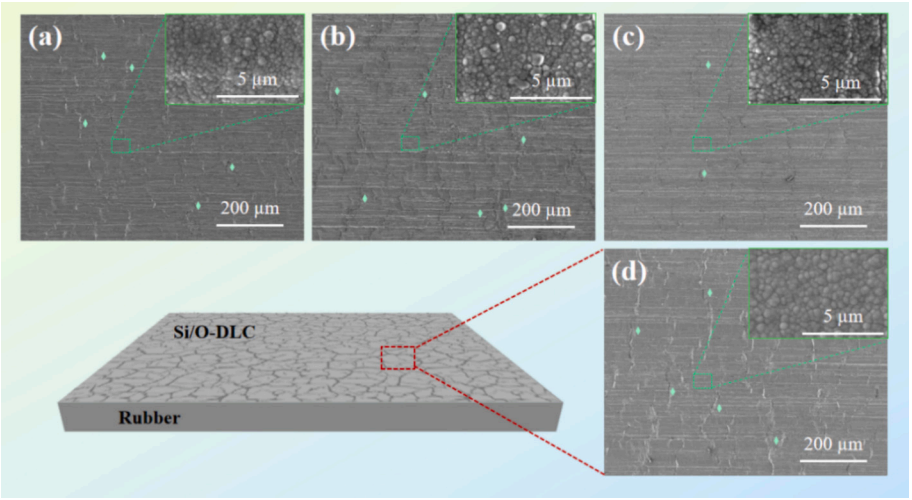

Fig. 4. Surface morphologies of DLC films on rubber (a) S0; (b) S1; (c) S2; (d) S3, insets in (a)–(d) are corresponding SEM images at high magnification (20000×) view.

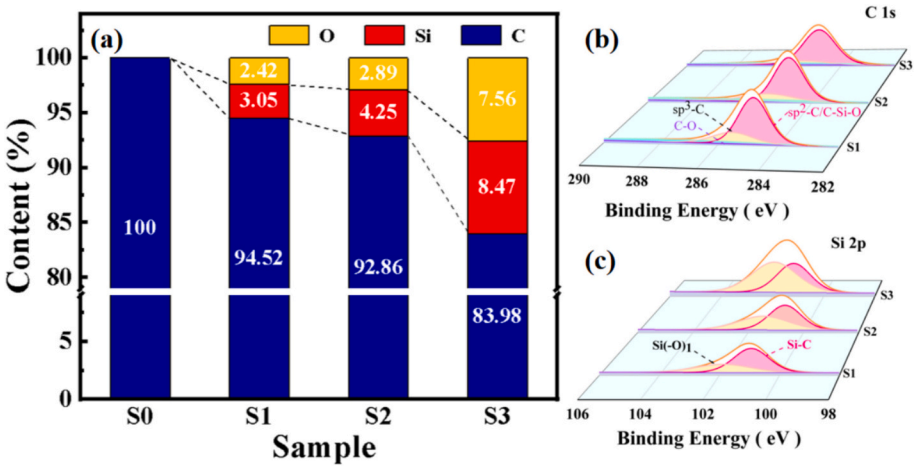

Fig. 5. (a) Chemical composition of films from XPS, and XPS high-resolution spectra of (b) C 1 s and (c) Si 2p.

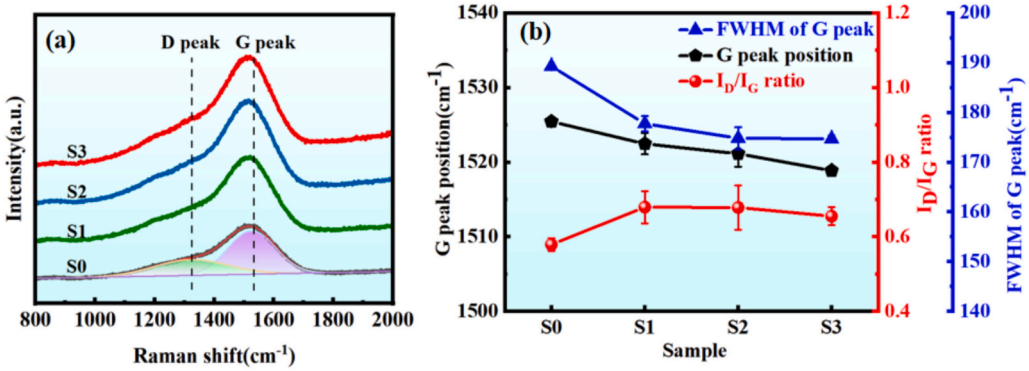

Fig. 6. (a) Raman spectra and (b) I_D/I_G, G peak position and FWHM of G peak of samples with various Si/O contents.

two main factors. First, the residual stress in S2 and S3 was significantly lower than that in S1 and S0. Second, S2 and S3 possessed lower hardness and modulus, resulting in better mechanical compatibility with the soft rubber substrate.

3.4. Flexibility evaluation with in-situ tensile testing

To evaluate the flexibility of the coated rubber, its surface morphology with different applied strain was investigated, as shown in Fig. 9 For S0, without applied strain in Fig. 9(a0), the surface exhibited some randomly distributed lattice of cracks, and the cracks were laid down perpendicular to the direction of the stripes. When the strain

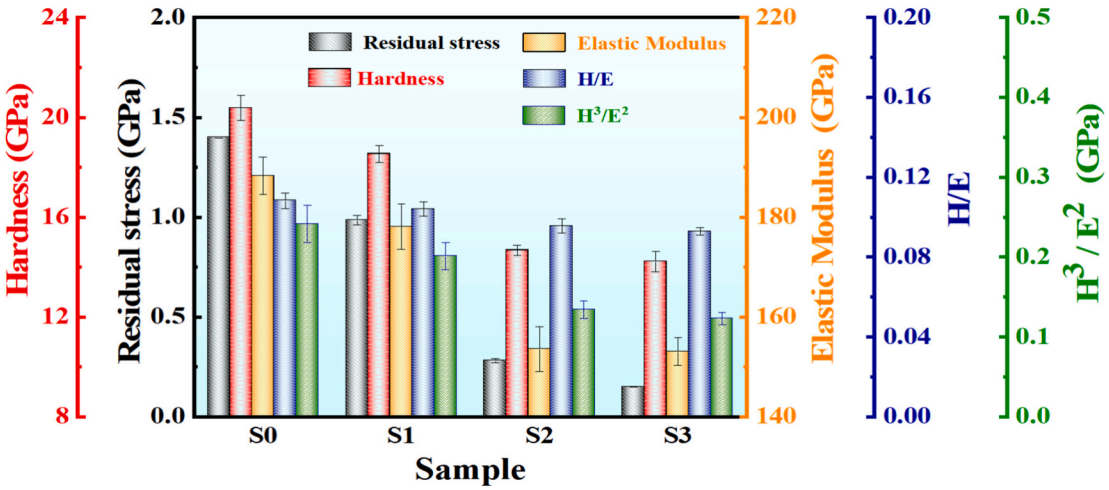

Fig. 7. Residual stress, Hardness, elastic modulus, H/E and $H^3/E^2$of DLC films on rubber with various Si/O contents.

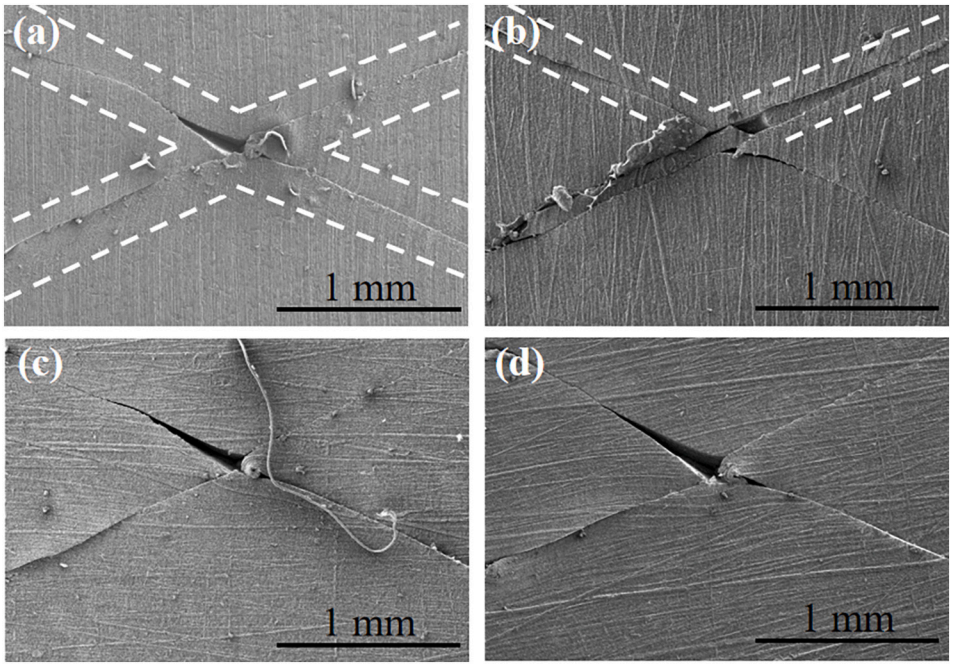

Fig. 8. SEM images of DLC films with different Si/O contents on rubber by X-cut test: (a) S0; (b) S1; (c) S2; (d) S3.

reached 5 %, the crack morphology began to change. As shown in Fig. 9 (b0), the gaps of the original cracks widen significantly, while more new cracks appeared in the regions marked by the blue triangles. As the strain increased to 10 %, as shown in Fig. 9(c0), the original cracks further expanded and new cracks continued to proliferate, causing the film to be segmented into smaller pieces. Simultaneously, delamination resulting from longitudinal contraction of the material became pronounced. As the strain was increased to 20 %, the cracks continued to widen, as depicted in Fig. 9(d0). At the higher strain level of 50 %, as shown in Fig. 9(e0), the crack gaps expanded to a maximum of 18.37 μm, while the crack density increased notably.

When the applied force was unloaded, the coated rubber can return back to its original length, as shown in Fig. 9(f0), the crack gap shrank to a smaller size, and some cracks generated during stretching can be clearly observed in Fig. 9(e0).

Fig. 9 (a1-f1) shows the surface morphology of S1 under different strains. Similarly, as stretching test proceeded, the existing cracks elongated, and new cracks began to grow around, the crack gap widened, and the crack lattice became finer and denser. After unloading and shrinking, the crack gap decreased, but the newly generated cracks can still remain on the surface, as marked by the yellow mark in Fig. 9 (f1). The results of in-situ tensile testing of S2 are shown in Fig. 9 (a2-f2), the original crack enlarged, up to 14.6 μm, new cracks were produced when stretching up to 10 %, after unloading and shrinking, the crack shrinkage became smaller, and new cracks produced during stretching basically disappeared. The surface morphology of S3 during stretching test is shown in Fig. 9(a3-f3). Compared with the previous three samples, with the increase of applied strain, the original crack extension phenomenon was delayed, and the maximum spacing of the cracks was only 8.67 μm, which was significantly reduced. After shrinkage, nearly all the new cracks produced during stretching disappeared.

Overall, no obvious film peeling occurred during stretching and unloading process for each sample, which indicated its high adhesion strength and good flexibility, with the increase of the Si/O content, the original crack expansion and new crack generation phenomenon of the films were significantly suppressed during the stretching process, and

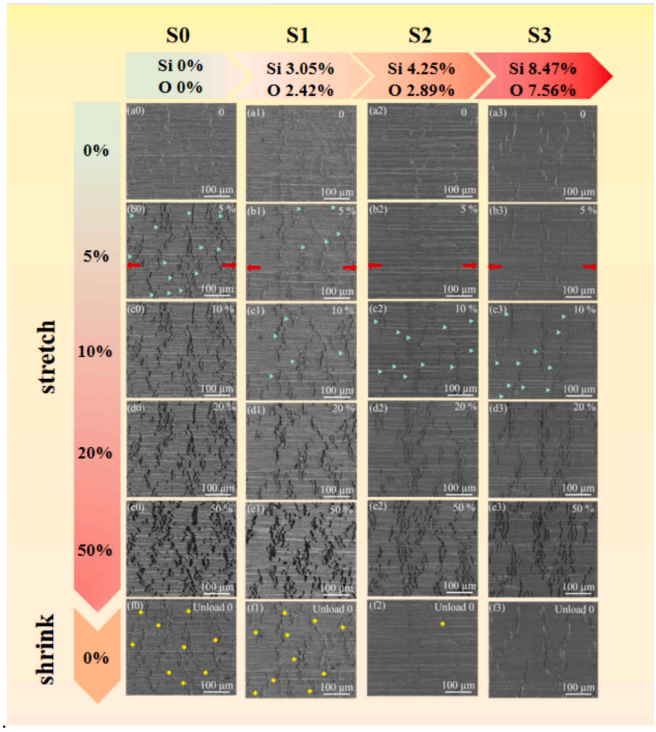

Fig. 9. Surface morphologies of DLC films with different Si/O contents under different strains: (a) 0 % (as-deposited), (b) 5 %, (c) 10 %, (d) 20 %, (e) 50 %, (f) 0 % (after unloading); the red arrow in the figure is the tensile direction. (For interpretation of the references to colour in this figure legend, the reader is referred to the web version of this article.)

the maximum crack spacing was reduced. After recovery from shrinkage, the crack healing effect was significantly improved. Clearly, with the increase of Si/O content, the decreased hardness and enhanced flexibility of the film can match the rubber substrate better.

3.5. Tribological properties

The COF curves of DLC coated rubber under 5 N are shown in Fig. 10 (a). The uncoated rubber substrate exhibited a relatively high COF, which increased further over the testing duration. For S0 and S1, their COF gradually increased from a starting value of 0.253 to 0.531 and from 0.252 to 0.455, respectively. This increase was attributed to the growing deformation of the rubber substrate under reciprocating normal load, which likely enhanced interface adhesion and consequently led to higher friction force over time. In comparison, the COF of S2 and S3 were consistently maintained at 0.267 ± 0.015 and 0.29 ± 0.023, respectively, showing excellent friction-reducing and lubricating properties.

From Fig. 10(b), under 10 N, the rubber showed the similar COF trend as that under 5 N. While, the COF of the coated samples changed greatly. The COF of S0 and S1 increased from the higher value of 0.310 at beginning to 1.111, and from 0.301 to 1.075, respectively. In contrast, S2 and S3 maintained relative more stable and lower COF at 0.377 and 0.322, respectively. Compared with rubber, the COF of S0 and S1 were close or higher. In consideration of excellent lubricating properties of DLC, the higher COF can be treated as the failure or severe wear of the DLC film. For S2 and S3, they had a higher COF at higher loads, but which was much lower than the rubber. This may be due to that the COF was mainly related to the interfacial shear strength and contact area. When the load increased, the actual contact area increased, so the COF increased accordingly.

Since S0 and S1 showed catastrophic failure at 10 N, the samples after tribological test at 5 N were selected to observe the surface morphology of the wear tracks, as shown in Fig. 11. For all samples, the width of the wear tracks was greater than 2 mm, which may be mainly influenced by the larger deformation of the rubber substrate during tribological test. For S0, its wear track was widest, and the cracks had the minimum size and maximum density. For S1 and S2, a denser crack network can be observed on the wear track. For S3, the abrasion marks were shallowest and the demarcation line was not obvious.

3.6. Stress distribution and deformation

During the friction testing process, the normal contact load will induce a heterogeneous stress field and multi-scale deformation response within the Si/O-DLC coated rubber system. First, as the Si/O content increased, the stress in DLC of the coated tended to decrease, maximum reduction of 15.6 % in stress , which can avoid stress concentration and suppress cracking and spalling, as shown in Fig. 9(a). And three typical regions should be concerned, as illustrated in Fig. 12(b), where regions I, II, and III stand for the maximum deformation zone, the intimate contact zone, and the contact separation zone, respectively. From von Mises stress distribution, the maximum stress magnitude of 1.56 GPa in the coating-substrate system was predominantly concentrated within region III, corresponding to the maximum curvature radius of the coating bending. This stress concentration phenomenon demonstrated direct correlation with the amplified strain gradient effect arising from modulus mismatch at the coating-substrate interface, namely, under large deformation of the compliant rubber substrate, the hard coating underwent localized buckling due to interfacial constraint,

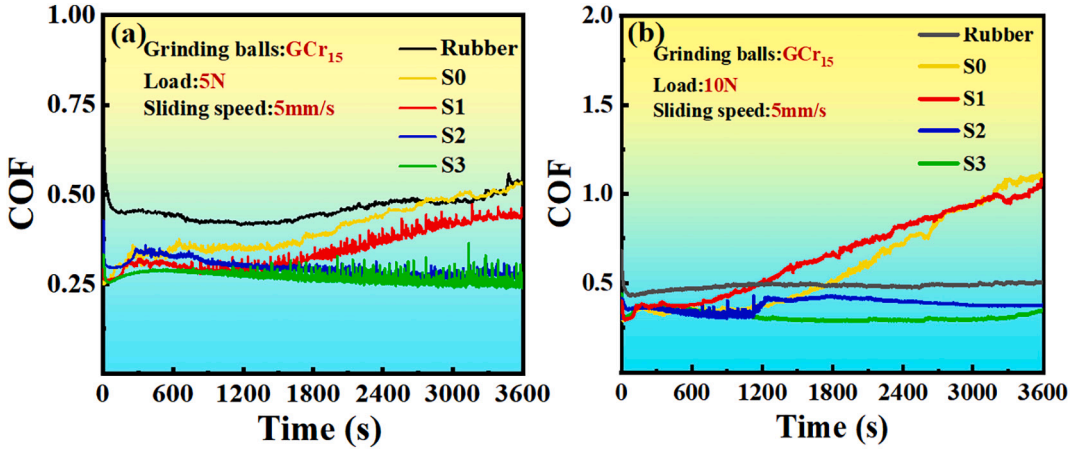

Fig. 10. The curves of friction coefficient of DLC films on rubber with different Si/O contents under (a) 5 N, and (b) 10 N.

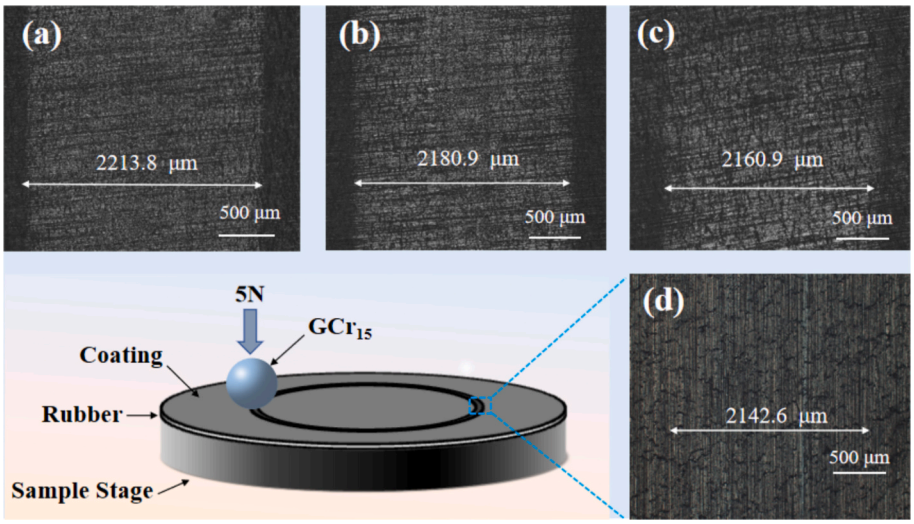

Fig. 11. Wear track morphologies of DLC under 5 N for (a) S0, (b) S1, (c) S2, (d) S3 samples.

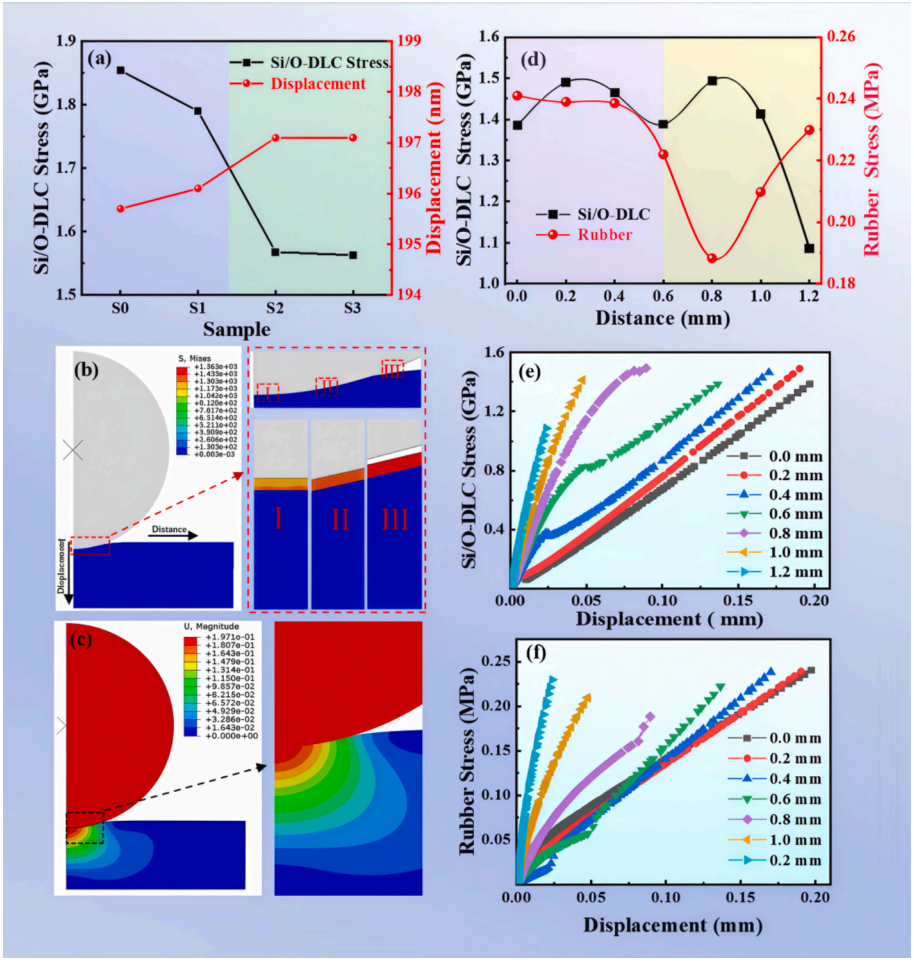

Fig. 12. (a) Stress and displacement diagram of S0-S3 coating, (b) Equivalent stress contours for S3 coated rubber. Regions I, II, and III are the magnified view of stress contours of the coating, (c) Deformation contours for S3 coated rubber and the magnified view, (d) Stress profiles of S3 coating and rubber substrate, (e) Stress-displacement diagram of S3 coating, (f) Stress-displacement diagram of rubber substrate at different distances from the axis.

leading to a significant restructuring of the in-plane principal stress state.

At the microscopic scale, the pronounced stress gradient distribution in the coating surface layer may facilitate interface debonding initiation. Macroscopically, the stress concentration zones exhibited strong spatial correlation with wear morphologies (e.g., plowing groove depth and spalling pit distribution). This cross-scale correlation can be quantitatively characterized through strain energy density distribution analysis,

in regions of maximum equivalent stress, once accumulated strain energy exceeded the fracture toughness threshold of the coating material, microcrack nucleation could initiate and ultimately lead to coating spalling.

Fig. 12(c). presents the deformation from S3 coated rubber systems. The maximum deformation occurred at the center of contact area between the ball and the coating, then decreased gradually with the distance away from the contact center, the maximum deformations of the S3 coated rubber were 0.2 mm in this case, with the corresponding maximum strain of 10 %.

To investigate the stress variation with deformation magnitude at distinct horizontal positions of the Si/O-DLC coating and rubber substrate during the loading process, the stress and displacement states of multiple nodes were recorded throughout the loading cycle, as illustrated in Fig. 12(d). The significant internal stress disparity under loading originated from the severe mechanical property mismatched between the two materials. During compressive loading, the compliant rubber substrate primarily underwent elastic deformation with extensive strain accommodation (The maximum substrate stress around 0.24 MPa), resulting in relatively low stress levels. In contrast, the S3 coating demonstrated pronounced stress concentration (The maximum coating stress around 1.56 GPa) due to its high elastic modulus and constrained bending deformation at the coating-substrate interface.

As depicted in Fig. 12(e) and (f), both the Si/O-DLC coating and rubber substrate demonstrated gradient-decreasing displacement magnitudes with increasing radial distance from the axial center, however, their stress distributions exhibited significant differences, the former displayed a non-monotonic characteristic of initial stress increase followed by a subsequent decrease in Fig. 12(e). The stress evolution in the Si/O-DLC coating primarily originated from bending deformation effects constrained by coating-substrate bonding. This geometric constraint induced notable stress concentration at interfacial regions, thereby causing localized stress intensification phenomena. In contrast, the stress evolution of the rubber substrate in Fig. 12(f) exhibited a characteristic of initial decrease followed by a subsequent increase. The stress recovery phenomenon was mainly attributed to coating-substrate interfacial coupling, bending deformation of the coating was transmitted through interfacial shear transfer, inducing a tensile stress field within adjacent regions of the rubber substrate, ultimately forming secondary stress concentration zones.

3.7. The possible wear mechanism under large deformation

Clearly, tribological performance of DLC-coated rubber can be analyzed from their elasticity, stress distribution and interfacial deformation characteristic under large deformation. Due to the significant mechanical mismatch between the flexible rubber substrate (Young' s modulus 0.001–0.1 GPa) and the hard DLC films (Young' s modulus >100 GPa), under a certain high normal load during tribological test, the compliant rubber substrate will undergo pronounced bending deformation. Meanwhile, the brittle Si/O-DLC films with higher modulus exhibited more crack initiation at the interface and even serious delamination. First, as the Si/O content increased, the stress in DLC, the hardness and elastic modulus of the coated rubber tended to decrease, as shown in Fig. 7(b), making it more compatible with the rubber substrate. Besides, the decrease in hardness and residual stress will also help to improve the adhesion strength between hard DLC and soft rubber, resulting in less cracks and delamination under large strains, as shown in the in-situ tensile testing in Fig. 9.

From the perspective of finite element analysis in Fig. 12, when constrained by the DLC/substrate interface, the DLC bending deformation induced by substrate deformation was significantly mitigated, thereby effectively suppressing the interfacial stress concentration effect. So the DLC-coated rubber exhibited a superior resistance to delamination and spalling under the similar loading conditions.

During the friction process, the largest hardness and elastic modulus of pure DLC film in Fig. 7 may cause severe spalling due to the large deformation, exhibiting increasing COF with longer test time in Fig. 10 and the widest wear track in Fig. 11. With increasing applied load from 5 N to 10 N, all the four coated samples exhibited a much larger COF. As for the S0 and S1 samples, their high brittleness caused severe cracking and premature failure.

Different from the S0 and S1 sample, the decreased hardness and enhanced flexibility of the S2 and S3 can match the rubber substrate better, as shown in in-situ tensile testing in Fig. 9, suggesting their significantly enhanced load-bearing capacity, which can significantly prevent bending deformation and following severe spalling. Simultaneously, by releasing stress to strengthen adhesion strength in Fig. 8, extensive cracking and spalling can be greatly suppressed under the tensile action of tangential friction force. In this case, the sliding interface exhibited enhanced stability, and interfacial contact behavior of the sliding system approximated the friction characteristics of rigid friction pairs, thereby exhibiting improved friction and wear characteristics of DLC. By comparison, both S2 and S3 samples had the higher Si and O content, the improved mechanical matching led to higher coating-substrate adhesion and enhanced interfacial deformation compatibility, result in less cracking, delamination, relatively stable and lower COF. The tribological process and wear mechanism of the silicon-oxygen co-doped DLC coated rubber are illustrated in Fig. 13.

4. Conclusion

In this work, Si/O-DLC films with different Si/O contents were deposited on nitrile rubber, where the effects of Si/O contents on the microstructure, adhesion strength, flexibility, and tribological behavior of DLC coated rubber were systematically investigated. The results showed that the doped Si and O content could be controlled from 3.05 to 8.47 at.% and from 2.42 to 7.56 at.%, respectively. With the increase of Si/O content in the DLC films, the sp^3 content was reduced, and the residual stress, the hardness as well as the elastic modulus showed a similar decreasing trend, while the adhesion strength was improved significantly. The higher Si/O content endowed the DLC films with decreased hardness and enhanced flexibility, which thereafter reduced mechanical mismatch between with Si/O-DLC film and the rubber substrate, holding larger deformation during tribological test. As a consequence, both the increased adhesion and good tribological behavior contributed the stable lower COF under 5 N and 10 N for rubber coated with Si/O-DLC films.

CRediT authorship contribution statement

Ziyu Du: Writing – original draft, Visualization, Validation, Investigation, Formal analysis, Data curation, Conceptualization. **Xin Zhang:** Writing – original draft, Visualization, Investigation, Formal analysis,

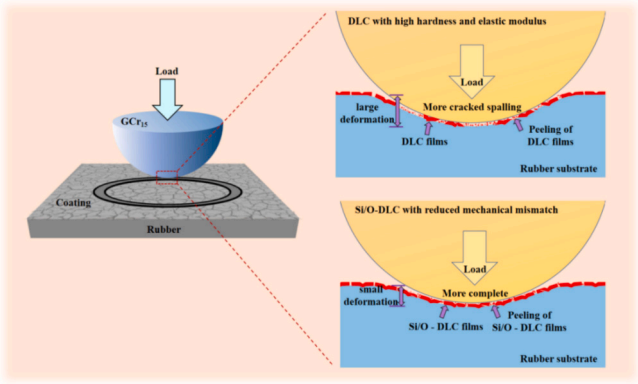

Fig. 13. The wear mechanism of Si/O-DLC coated rubber.

Data curation. **Silong Zhang:** Validation, Data curation. **Rende Chen:** Methodology, Investigation. **Wei Yang:** Investigation, Data curation. **Hao Li:** Writing – review & editing. **Kazuhito Nishimura:** Methodology, Investigation. **Peng Guo:** Writing – review & editing, Visualization, Project administration, Investigation, Funding acquisition, Conceptualization. **Aiying Wang:** Writing – review & editing, Visualization, Resources, Project administration, Funding acquisition.

Declaration of competing interest

The authors declare that they have no known competing financial interests or personal relationships that could have appeared to influence the work reported in this paper.

Data availability

Data will be made available on request.

Acknowledgements

This work was financially supported by National Science Foundation of China (U24A2030, 52127803), Leading Innovative and Entrepreneur Team Introduction Program of Zhejiang (2024R01004), Zhejiang Lingyan Research and Development Program (2024C01159), and Major Special Project of Ningbo (2024Z134). The authors wish to thank the assistance of Xianchun Jiang and Lingkang Meng at School of Mechanical Science and Engineering, Huazhong University of Science and Technology for FEM discussion.

References

[1] A.M. Wemyss, C. Bowen, C. Plesse, C. Vancaeyzeele, G.T.M. Nguyen, F. Vidal, C. Wan, Dynamic crosslinked rubbers for a green future: a material perspective, Mater. Sci. Eng. R 141 (2020), https://doi.org/10.1016/j.mser.2020.100561.

[2] Y. Ma, L. Wu, C. Li, X. Meng, X. Peng, J. Jiang, Thermal-mechanical-diffusion multi-field coupling behavior of rubber seals in high-pressure hydrogen environment, Int. J. Hydrogen Energy 112 (2025) 333–346, https://doi.org/10.1016/j.ijhydene.2025.02.390.

[3] Y.T. Pei, X.L. Bui, J.P. van der Pal, D. Martinez-Martinez, X.B. Zhou, J.T.M. De Hosson, Flexible diamond-like carbon films on rubber: on the origin of self-acting segmentation and film flexibility, Acta Mater. 60 (2012) 5526–5535, https://doi.org/10.1016/j.actamat.2012.07.017.

[4] H. Bhaskaran, B. Gotsmann, A. Sebastian, U. Drechsler, M.A. Lantz, M. Despont, P. Jaroenapibal, R.W. Carpick, Y. Chen, K. Sridharan, Ultralow nanoscale wear through atom-by-atom attrition in silicon-containing diamond-like carbon, Nat. Nanotechnol. 5 (2010) 181–185, https://doi.org/10.1038/nnano.2010.3.

[5] X. Li, A. Wang, K.-R. Lee, Fundamental understanding on low-friction mechanisms at amorphous carbon interface from reactive molecular dynamics simulation, Carbon 170 (2020) 621–629, https://doi.org/10.1016/j.carbon.2020.08.014.

[6] J. Wei, P. Guo, L. Liu, H. Li, H. Li, S. Wang, P. Ke, H. Saito, A. Wang, Corrosion resistance of amorphous carbon film in 3.5 wt% NaCl solution for marine application, Electrochim. Acta 346 (2020), https://doi.org/10.1016/j.electacta.2020.136282.

[7] X. Zhou, Y. Zhang, P. Guo, L. Cui, A. Wang, P. Ke, Tribological behavior of Cr/a-C multilayered coating against PEEK under dry sliding condition, Wear 518-519 (2023), https://doi.org/10.1016/j.wear.2023.204625.

[8] L. Qiang, S. Yu, G. Liu, H. Tang, X. Zhang, J. Zhang, Comparative study on the influence of bias on the properties of Si-DLC film with and without Si interlayer on NBR: the role of Si interlayer, Diamond Relat. Mater. 101 (2020), https://doi.org/10.1016/j.diamond.2019.107614.

[9] J.Q. Liu, L.J. Li, B. Wei, F. Wen, H.T. Cao, Y.T. Pei, Effect of sputtering pressure on the surface topography, structure, wettability and tribological performance of DLC films coated on rubber by magnetron sputtering, Surf. Coat. Technol. 365 (2019) 33–40, https://doi.org/10.1016/j.surfcoat.2018.05.012.

[10] E.L. Dalibón, L. Escalada, S. Simison, C. Forsich, D. Heim, S.P. Brühl, Mechanical and corrosion behavior of thick and soft DLC coatings, Surf. Coat. Technol. 312 (2017) 101–109, https://doi.org/10.1016/j.surfcoat.2016.10.006.

[11] Y.M. Wu, J.Q. Liu, H.T. Cao, Z.Y. Wu, Q. Wang, Y.P. Ma, H. Jiang, F. Wen, Y.T. Pei, On the adhesion and wear resistance of DLC films deposited on nitrile butadiene rubber: a Ti-C interlayer, Diamond Relat. Mater. 101 (2020), https://doi.org/10.1016/j.diamond.2019.107563.

[12] S. Thirumalai, A. Hausberger, J.M. Lackner, W. Waldhauser, T. Schwarz, Effect of the type of elastomeric substrate on the microstructural, surface and tribological characteristics of diamond-like carbon (DLC) coatings, Surf. Coat. Technol. 302 (2016) 244–254, https://doi.org/10.1016/j.surfcoat.2016.06.021.

[13] C. Bai, L. Qiang, B. Zhang, K. Gao, J. Zhang, Optimizing the tribological performance of DLC-coated NBR rubber: the role of hydrogen in films, Friction 10 (2021) 866–877, https://doi.org/10.1007/s40544-021-0498-0.

[14] C. Han, T. Yang, X. Lin, Y. Song, M. Xie, Q. Deng, F. Wen, Effect of bias gradient delta on mechanical and tribological properties of DLC films sputtered on ACM, Surf. Coat. Technol. 481 (2024), https://doi.org/10.1016/j.surfcoat.2024.130626, 130626-.

[15] R. Matsumoto, K. Sato, K. Ozeki, K. Hirakuri, Y. Fukui, Cytotoxicity and tribological property of DLC films deposited on polymeric materials, Diamond Relat. Mater. 17 (2008) 1680–1684, https://doi.org/10.1016/j.diamond.2008.02.027.

[16] Y.T. Pei, X.L. Bui, J.P. van der Pal, D. Martinez-Martinez, J.T.M. De Hosson, Flexible diamond-like carbon film coated on rubber, Prog. Org. Coat. 76 (2013) 1773–1778, https://doi.org/10.1016/j.porgcoat.2013.05.015.

[17] M. Lubwama, B. Corcoran, K.V. Rajani, C.S. Wong, J.B. Kirabira, A. Sebbit, K. A. McDonnell, D. Dowling, K. Sayers, Raman analysis of DLC and Si-DLC films deposited on nitrile rubber, Surf. Coat. Technol. 232 (2013) 521–527, https://doi.org/10.1016/j.surfcoat.2013.06.013.

[18] M. Lubwama, B. Corcoran, K.A. McDonnell, D. Dowling, J.B. Kirabira, A. Sebbit, K. Sayers, Flexibility and frictional behaviour of DLC and Si-DLC films deposited on nitrile rubber, Surf. Coat. Technol. 239 (2014) 84–94, https://doi.org/10.1016/j.surfcoat.2013.11.023.

[19] N.M.R. Shah, J. Song, C.-D. Yeo, Thermomechanical properties and frictional contact behavior of oxygen doped DLC film through molecular dynamics simulation, Diamond Relat. Mater. 120 (2021), https://doi.org/10.1016/j.diamond.2021.108653.

[20] D. Zhang, S. Li, X. Zuo, P. Guo, P. Ke, A. Wang, Structural and mechanism study on enhanced thermal stability of hydrogenated diamond-like carbon films doped with Si/O, Diamond Relat. Mater. 108 (2020), https://doi.org/10.1016/j.diamond.2020.107923.

[21] X. Jiang, P. Guo, L. Cui, Y. Zhang, R. Chen, Y. Ye, A. Wang, P. Ke, Tribological behavior of silicon and oxygen co-doped hydrogenated amorphous carbon coatings on polyether ether ketone, Diamond Relat. Mater. 132 (2023), https://doi.org/10.1016/j.diamond.2022.109650.

[22] L. Cui, P. Guo, X. Zhou, S. Zhu, P. Ke, A. Wang, The mechanical and tribological properties of polyether ether ketone coated by diamond-like carbon film with plasma-induced transition layer, Diamond Relat. Mater. 147 (2024), https://doi.org/10.1016/j.diamond.2024.111345, 111345–111345.

[23] Y.T. Pei, D. Martinez-Martinez, J.P.v.d. Pal, X.L. Bui, X.B. Zhou, J.T.M.D. Hosson, Flexible diamond-like carbon films on rubber: friction and the effect of viscoelastic deformation of rubber substrates, Acta Mater. 60 (2012) 7216–7225, https://doi.org/10.1016/j.actamat.2012.09.031.

[24] P.S. Phani, W.C. Oliver, G.M. Pharr, Understanding and modeling plasticity error during nanoindentation with continuous stiffness measurement, Mater. Des. 194 (2020), https://doi.org/10.1016/j.matdes.2020.108923.

[25] J.Q. Liu, Z.Y. Wu, H.T. Cao, F. Wen, Y.T. Pei, Effect of bias voltage on the tribological and sealing properties of rubber seals modified by DLC films, Surf. Coat. Technol. 360 (2019) 391–399, https://doi.org/10.1016/j.surfcoat.2018.12.100.

[26] J. Cao, Z. Yin, H. Li, G. Gao, Tribological studies of soft and hard alternated composite coatings with different layer thicknesses, Tribol. Int. 110 (2017) 326–332, https://doi.org/10.1016/j.triboint.2017.02.039.

[27] C.A. Griffiths, A. Rees, R.M. Kerton, O.V. Fonseca, Temperature effects on DLC coated micro moulds, Surf. Coat. Technol. 307 (2016) 28–37, https://doi.org/10.1016/j.surfcoat.2016.08.034.

[28] Y. Isono, T. Namazu, N. Terayama, Development of AFM tensile test technique for evaluating mechanical properties of sub-micron thick DLC films, J. Microelectromech. Syst. 15 (2006) 169–180, https://doi.org/10.1109/jmems.2005.859196.

[29] Shuyu L., Hao L., Guanshui M., Jing W., Guangxue Z., Yan Z., Peng G., Peiling K., Aiying W., Dense Cr/GLC multilayer coating by HiPIMS technique in high hydrostatic pressure: microstrusctural evolution and galvanic corrosion failure, Corros. Sci. 225 (2023), https://doi.org/10.1016/j.Corsci.2023.111618.

[30] H. Shangyang, Y. Haodong, W. Zhanjiang, Comparative study on several constitutive models of GCr15 steel at high strain rates, J. Mater. Eng. Perform. 33 (2023) 1797–1815, https://doi.org/10.1007/s11665-023-08092-0.

[31] Q. Zhang, J.W. Shi, S.F. Suo, G.Y. Meng, Finite element analysis of rubber materials based on Mooney - Rivlin models and Yeoh models, China Synth. Rubber Ind. 43 (2020) 468–471, https://doi.org/10.3969/j.issn.1000-1255.2020.06.006.

[32] Y.T. Pei, X.L. Bui, J.T.M. De Hosson, Deposition and characterization of hydrogenated diamond-like carbon thin films on rubber seals, Thin Solid Films 518 (2010) S42–S45, https://doi.org/10.1016/j.tsf.2010.03.018.

[33] D. Martinez-Martinez, J.T.M. De Hosson, On the deposition and properties of DLC protective coatings on elastomers: a critical review, Surf. Coat. Technol. 258 (2014) 677–690, https://doi.org/10.1016/j.surfcoat.2014.08.016.

[34] L.-A. O'Hare, B. Parbhoo, S.R. Leadley, Development of a methodology for XPS curve-fitting of the Si 2p core level of siloxane materials, Surf. Interface Anal. 36 (2004) 1427–1434, https://doi.org/10.1002/sia.1917.

[35] M. Lubwama, B. Corcoran, K. Sayers, J.B. Kirabira, A. Sebbit, K.A. McDonnell, D. Dowling, Adhesion and composite micro-hardness of DLC and Si-DLC films

deposited on nitrile rubber, Surf. Coat. Technol. 206 (2012) 4881–4886, https://doi.org/10.1016/j.surfcoat.2012.05.079.
[36] H. Lan, T. Kato, C. Liu, Molecular dynamics simulations of atomic-scale tribology between amorphous DLC and Si-DLC films, Tribol. Int. 44 (2011) 1329–1332, https://doi.org/10.1016/j.triboint.2010.10.006.
[37] M. Ban, T. Hasegawa, Internal stress reduction by incorporation of silicon in diamond-like carbon films, Surf. Coat. Technol. 162 (2003) 1–5, https://doi.org/10.1016/S0257-8972(02)00572-8.